Batteries & Supercaps

Research Article
doi.org/10.1002/batt.202300498

Chemistry Europe
European Chemical Societies Publishing

www.batteries-supercaps.org

One-step Surface-to-bulk Modification of $NaCrO_2$ Cathode for Durable Sodium-ion Batteries

Chen Chen,[a] Yingbin Hong,[a] Baolong Liang,[a] Yiyin Huang,[a] Mingdeng Wei,[b] Hu-Rong Yao,[a] Lituo Zheng,*[a] and Zhensheng Hong*[a, c]

$NaCrO_2$ is a promising O3-type cathode material in sodium-ion batteries. However, it suffers from rapid capacity fading due to the unstable structure upon cycling. This work shows that *in situ* carbon coating during the synthesis process has multiple synergistic effects and can effectively stabilize the material structure and improve the cyclability. It is found that sodium vacancy and carbon coating in $NaCrO_2$ synchronously occur, which improve its sodium-ion transport kinetics, structural stability during cycling and the air stability. More importantly, the strategy is universal in that various sources of carbon display similar effect. As a result, the asphalt-derived carbon coated material has a high initial capacity of 129 mAh g^{-1} at 0.1 C rate with an initial Coulombic efficiency up to 98.2%. In addition, it shows an excellent rate capability and cycling performance with 81.1% retention after 1000 cycles at 5 C in half cell. Moreover, a full cell has constructed by coupling with hard carbon anode, which shows a high discharge capacity of 121.9 mAh g^{-1} with a high Coulomb efficiency of 94.7%, excellent rate capability and good cycling stability. This work demonstrates a general modification method on $NaCrO_2$ that has the potential for practical applications.

Introduction

With the fast development of electric vehicles (EVs) and portable mobile devices, higher requirements are put forward for efficient and cost-effective energy storage systems. Lithium-ion batteries (LIBs) could face the problem of resource depletion.[1–3] In response to this issue, attempts have been made to develop sodium-ion batteries (SIBs) as a possible alternative to LIBs energy storage systems. Sodium and lithium have similar electrochemical properties, and sodium has advantages such as abundant resources, environmental friendliness and low price.[4–6] The percentage of sodium in the earth's crust by mass is 2.64%, while the lithium content is only 0.0065%.[7,8] Therefore SIBs are considered promising as the next generation of energy storage batteries.

Layered oxide materials are currently regarded as one of the most promising cathode materials for sodium ion batteries.[9–11] There are two most common types of Na-based layered transition metal oxides Na_xMO_2, namely the O3 type and P2 type. O and P represent Na occupying the octahedral and prismatic sites formed by oxygen respectively, while the number represents the stacking layers of sodium in a unit cell.[12,13] Compared with P2-type positive electrode, O3 layered positive electrode has higher sodium content and can provide more recyclable sodium.[14] $NaCrO_2$ is a classical O3-type layered positive electrode material. When the battery is charging or discharging, this material undergoes complex phase transitions and new phases such as O'3 and P3 can be formed.[15–18] These structural changes lead to poor cycle stability. In addition, $NaCrO_2$ is less stable in air because the Na in the material get exchanged by protons and H_3O^+.[19] The decrease of sodium content and the change of structure increase the interfacial resistance, which leads to the decrease of stability.[20]

Element doping and surface coating are two methods that have been proved to be effective in improving stability.[21] It has been reported that doping of Ca can improve material disorder, smooth voltage curves, improve cyclability and air stability at a cost of reduced capacity.[22,23] Elemental substitution of transition metal sites is also an effective strategy. It has been reported that Ti–O bonds are stronger than Cr–O bonds, thus slowing the O3–P3 phase transition and increasing the operating voltage.[24] Manganese, as a cheap metal, has also been used in doping. It has been found that $NaCr_{0.8}Mn_{0.2}O_2$ material has higher average storage voltage than $NaCrO_2$ material. In addition, manganese substitution leads to an improved capacity retention rate of 98% after 100 cycles at 0.1 C current density.[25] An earlier study of $NaCrO_2$ surface coating using citric acid as a carbon source showed that the coating provided significantly improved electrochemical stabil-

[a] C. Chen, Y. Hong, B. Liang, Prof. Y. Huang, Prof. H.-R. Yao, Dr. L. Zheng, Prof. Z. Hong
Fujian Provincial Key Laboratory of Quantum Manipulation and New Energy Materials
College of Physics and Energy
Fujian Normal University
Fuzhou, Fujian 350117 (China)
E-mail: zhenglituo@fjnu.edu.cn
zshong@fjnu.edu.cn

[b] M. Wei
Fujian Provincial Key Laboratory of Electrochemical Energy Storage Materials
Fuzhou University
Fuzhou, Fujian, 350116 (China)

[c] Prof. Z. Hong
Academy of Carbon Neutrality of Fujian Normal University
Fuzhou, 350117 (China)

Supporting information for this article is available on the WWW under https://doi.org/10.1002/batt.202300498

ity over the raw material.[26] Subsequently, Bhardwaj et al.[27] produced core-shell $NaCrO_2$/C by thermochemical treatment of C_2H_2. The carbon shell improves conductivity of the cathode material and helps to reduce adverse reactions at the electrode and electrolyte interface because it prevents the direct exposure of the cathode material to the electrolyte. In addition, Wang et al. accidentally found that Cr_2O_3, often considered as an impurity in electrode materials, provides excellent long cycle stability when applied as a coating material. Under a current density of 10 C, after 1000 cycles, it still has a specific capacity of 100.4 mAh g^{-1} with a retention rate of about 84.8%.[28] On this basis, Ikhe et al.[29] combined Cr_2O_3 coating with Al doping and found that the specific capacity had almost no attenuation after 1000 cycles. All the above studies show that surface coating is a very useful strategy to improve the stability of materials. In addition, *in situ* construction of oxygen vacancies has also been successfully reported by researchers.[30] Moreover, Zhou et al.[31,32] developed a series of corrugated layered structure and microcube structure adjustment in the layered positive electrode of potassium ion batteries, which provide a new materials design practice for material modification.

In this work, we report an asphalt/$NaCrO_2$ material (P@NCO) and explore the effects of different proportions of asphalt on material properties. X-ray photoelectron spectroscopy (XPS) analysis, thermogravimetric (TG) analysis and transmission electron microscopy (TEM) were used to analyze the coated carbon quantitatively and qualitatively on the surface of $NaCrO_2$ particles. We confirm that P@NCO has excellent electrochemical performance compared to bare-$NaCrO_2$ in terms of cyclic stability and rate capability. In order to increase the practicality of the material, we used the coated material with hard carbon anode electrode to assemble Na full cells. The result shows that it is a simple and feasible method to use asphalt as carbon source to coat $NaCrO_2$, which can improve the electrochemical performance and structure stability.

Results and Discussion

Structural characterization

The crystal structure of synthesized materials were characterized by XRD. It can be seen in Figure 1(a) that the asphalt coating does not change the crystal structure of the $NaCrO_2$ (NCO). As shown in the enlarged region of (003) peak, the diffraction peak of three coated-materials (*x*%P@NCO) slightly shift to lower angle, indicating that the addition of asphalt increases layer spacing.[33] Rietveld refinement were conducted on all samples and the obtained data were summarized in Table S1 and visualized in Figure 1(b). With increasing asphalt added, the lattice constant *c* increases while the sodium content decreases. Pristine NCO sample has a sodium content around 1.00 according to Rietveld refinement, while a sodium content of 0.98, 0.98, and 0.99 were obtained for 2%P@NCO, 4%P@NCO, and 6%P@NCO, respectively. This is because during sintering process, some sodium can be taken away by the decomposition and evaporation of asphalt compound. The reduction of positively charged Na^+ increases the electrostatic repulsion of negatively charged oxygen ions in adjacent layers, leading to the lattice expansion,[34–36] and thus providing a wider

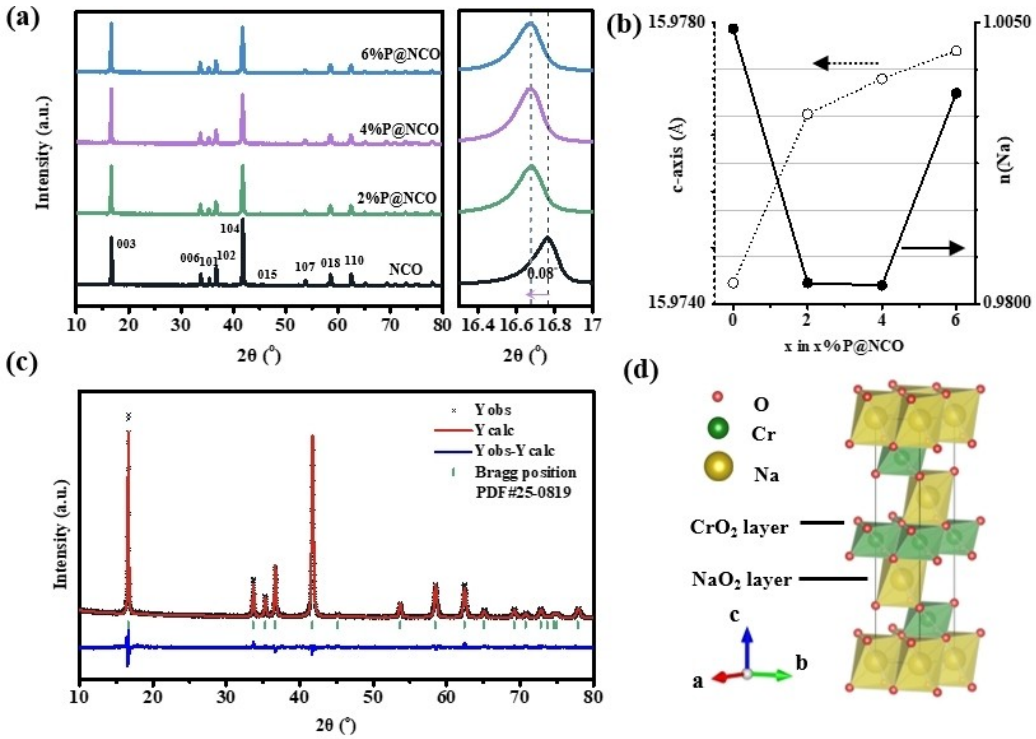

Figure 1. a) XRD patterns of NCO, 2%P@NCO, 4%P@NCO, 6%P@NCO samples, b) evolution of lattice constants and sodium content with×in *x*%P@NCO obtained from the refinements, c) Rietveld refinements for XRD pattern of 4%P@NCO, d) schematic diagram of O3 layer-type oxide crystal structure.

ionic path for the transport of Na^+. When the amount of asphalt further increases to 6%, the sodium content become higher, indicating that excessive coating carbon might prevent the loss of Na. The effect of various sources of carbon was also investigated. After modifying NCO with citric acid (CA@NCO) and vitamin C (Vc@NCO), as shown in the Figure S1 and Table S1, both materials exhibit a decrease in sodium content similar to *x*%P@NCO. In order to further confirm the reduction of sodium content caused by carbon combustion, the Na:Cr ratio obtained by ICP-OES is shown in Table S2. It is found that when the coating amount is 4%, the Na:Cr ratio showed the lowest results is 0.92:1. Therefore, the *in situ* asphalt modification method not only provides a carbon coating on the surface, but also creates sodium vacancies in the crystal structure, which could lead to better battery performance.[34,37] Figure 1(c) shows the Rietveld refinement pattern of 4%P@NCO material, where all the diffraction peaks can be well indexed to O3–$NaCrO_2$ (JCPDS card no. PDF#25-0819, space group = R-3 m). The positions of Na, O, and Cr atoms in the O3 crystal structure are shown in Figure 1(d). Table 1 shows the obtained lattice parameters from Rietveld refinement for the four samples.

The micromorphological character of the samples were characterized by scanning electron microscope (SEM). As shown in Figure 2(a–d), it can be seen that x%P@NCO are composed of stacked nanosheets with multilayer orientation, and this phenomenon becomes more obvious when the×value increases, which is of great significance for shortening the transport channel of sodium ions.[38,39] This unique structure was not observed in raw NCO material, suggesting that asphalt coating contributes to morphological regulation. In order to further observe the morphology and coating of the materials, high-resolution transmission electron microscopy (HRTEM) and selected area electron diffraction (SAED) were conducted on 4%P@NCO powder. Figure 2(e) shows that NCO was successfully coated with a carbon layer of nanometer thickness. The SAED image inserted in Figure 2(e) shows that all d-spacings derived can well correspond to O3-type materials. As shown in Figure 2(f), lattice fringes can be clearly observed. The measured d-spacing is about 0.543 nm, consistent with the crystal plane (003) of NCO obtained by Rietveld refinement.

In order to further verify the state of carbon element on the surface of the four materials, XPS (Figure 2g) was conducted and the coexistence of Na, Cr, O and C elements were confirmed. The spectra of Na_{1s} and C_{1s} are shown in Figure 2(h and i). Na_{1s} spectra show that carbon coating significantly affect the existence form of sodium element.[40] Cr_{2p} spectra show in Figure S2. C_{1s} spectra exhibit that carbon content increases with the adding of more asphalt, which confirms the successful coating on NCO. In order to further affirm this result, Thermogravimetric Analysis (TGA) were carried out on the material at 900 °C, and the result is shown in Figure S3. The pattern shows NCO weight change of 11.31% is close to the theoretical value of 11.2%.[41] And the carbon content of 4% P@NCO material is calculated to be 1.42% (12.73–11.31%) which proves the successful asphalt modification.[27] As shown in Figure 2(j), O_{1s} partial peak fitting are performed for the XPS data of NCO and 4%P@NCO. The peaks located in 528.9 eV, 531.0 eV, 532.9 eV and 534.7 eV be interpreted as lattice oxygen, oxygen vacancies (O_{vac}), chemisorbed oxygen and Na KLL Auger, respectively.[30,42–44] According to the above, chemisorbed oxygen on the material surface increases the resistance and leads to capacity fading. However, the addition of asphalt reduces chemisorbed oxygen on the surface of materials, which means carbon coating can improve air stability of $NaCrO_2$. To verify the decrease of chemisorbed oxygen of NCO, FTIR technology was used to analyze the functional group of NCO and 4%P@NCO (Figure 2k). The peaks located on 521 cm^{-1} and 914 cm^{-1} were corresponding to the Cr–O bond. The peak at 1444 cm^{-1} be thought to the Na–O bond. The vibration peaks at 3424 cm^{-1} which corresponds to O–H stretching vibration of $NaCrO_2$.[45] The difference is that 4%P@NCO material does not have O–H vibration peak, but has the characteristic peak of C–H bond due to the carbon coating. Overall, it observed that the asphalt compound modification can regulate the surface and bulk structure as well as particle morphology. These features are favorable for electrochemical performance, which we will discuss in the later text.

Electrochemical performance

The electrochemical performance of NCO and asphalt treated samples were studied using coin-type half cells. Figure 3(a) shows the initial charge and discharge curves of different samples at 0.1 C (1 C = 100 mA g^{-1}) in the voltage range of 2.0–3.6 V. NCO, 2%P@NCO, 4%P@NCO and 6%P@NCO show specific capacities of 119.2, 119.4, 128.9, and 111.1 mAh g^{-1}, respectively. Among these samples, 4% was found to be the best asphalt coating ratio, providing additional specific capacity for the material while significantly improving cycle stability. This is due to the fact that the surface coating improves the stability of the interface and inhibits the irreversible phase change of the material.[46] At the same time, it is worth noting that ICE of 4%P@NCO is 98.2%, which is higher than 97.6% of NCO, indicating that surface coating can prevent the direct reaction between bare electrode surface and electrolyte, and reduce the

Table 1. Calculated lattice parameters from Rietveld refinements of NCO, 2%P@NCO, 4%P@NCO and 6%P@NCO.

Materials	*a* [Å]	*c* [Å]	R_{wp}	χ^2	*n*(Na)
NCO	2.97580	15.97440	8.54%	2.042	1.00445
2%P@NCO	2.97560	15.97680	7.61%	1.768	0.98187
4%P@NCO	2.97530	15.97720	7.84%	1.874	0.98165
6%P@NCO	2.97560	15.97890	7.61%	1.784	0.99873

Research Article
doi.org/10.1002/batt.202300498
Chemistry Europe
European Chemical Societies Publishing

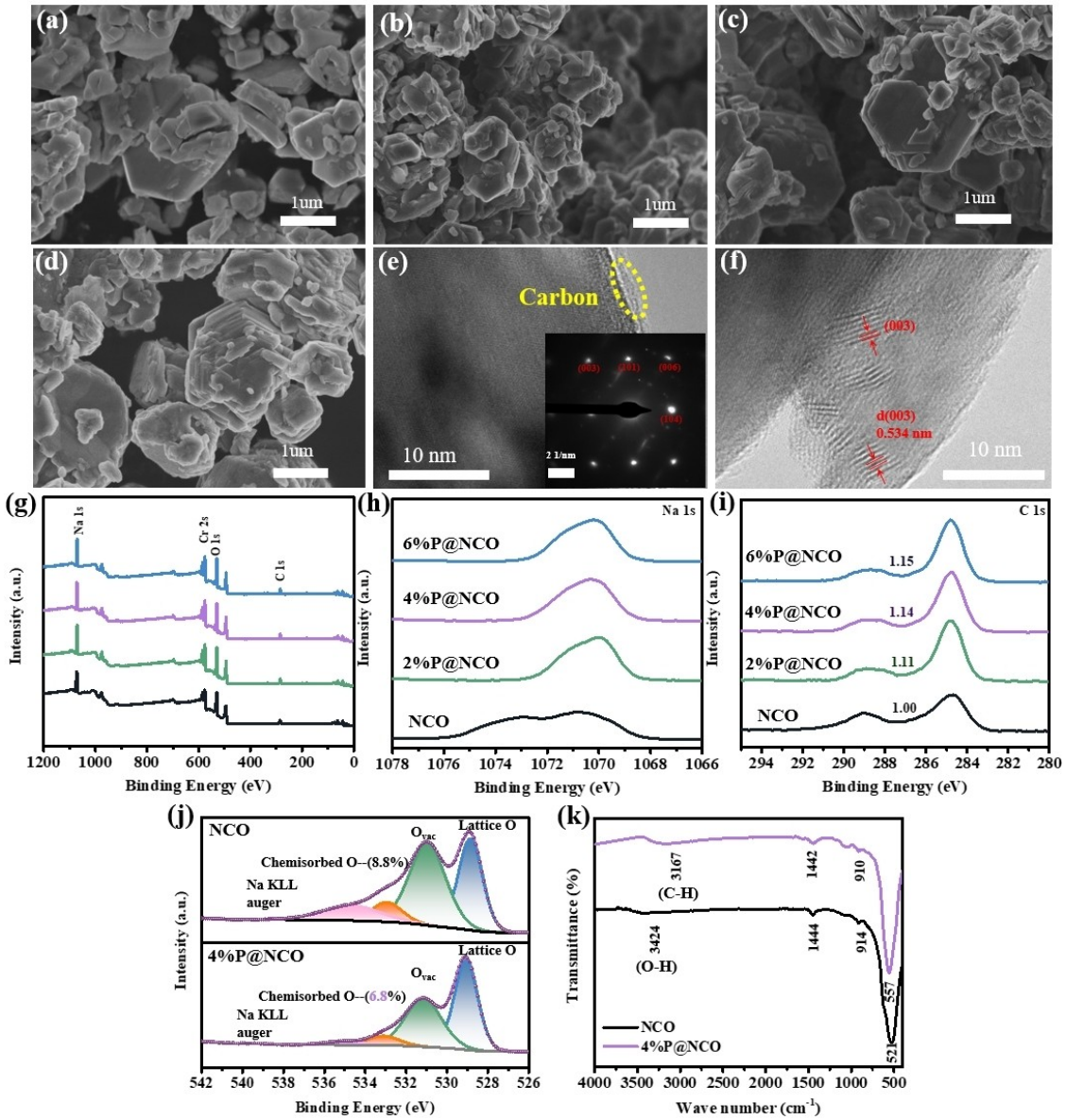

Figure 2. SEM image of a) bare $NaCrO_2$, b) 2%P@NCO, c) 4%P@NCO and d) 6%P@NCO. e and f) HRTEM image of 4%P@NCO and the SAED pattern of 4% P@NCO were inserted. g) XPS survey of NCO and *x*%P@NCO. XPS spectra of h) Na 1s, and i) C 1s and j) O 1s. k) FTIR spectra of prepared layered NCO and 4% P@NCO.

decomposition of electrolyte and other side reactions. This is beneficial for the sodium de/intercalation kinetics in charge/discharge process.[47,48] Figure 3(b) shows that rate performance of materials are greatly improved, especially under high current density of 50 C. The corresponding charge/discharge curves of different samples are shown in Figure S4. The 4%P@NCO sample tested at 0.1 C, 0.5 C and 1 C and 5 C, 10 C, 20 C and 50 C show excellent specific capacity of 126.5, 124.9, 124.2, 122.5, 120.8, 114.7 and 78.4 mAh g^{-1}. 4%P@NCO material in Figure 3(c and d) shows obvious improvement in cycling performance, and the Coulombic efficiency is more stable for coated material than that of raw NCO. The charge/discharge curves of NCO and 4%P@NCO at different cycle numbers were compared in Figure 3(e and f). The capacity retention rate of 4%P@NCO is 92.5% after 200 cycles, while the retention rate of NCO is only 61.2%.

The long term cycling performance of 4%P@NCO in shown in Figure 3(g), where the material can maintain a remarkable capacity retention of 81.1% after 1000 cycles at 5 C. The comparison pattern with the 5 C long cycles of the other two materials is shown in Figure S5. In addition, the electrochemical performance of citric acid and vitamin C modified materials is shown in Figure S6, proving the universality of the strategy in improving the cycling performance.

Figure 4(a and b) displays the cyclic voltammogram (CV) curves in the voltage range of 2–3.6 V of the four samples measured at a scan rate of 0.1 mV s^{-1} and 1 mV s^{-1}, respectively. Two pairs of redox peaks are clearly observed at 3.12/2.72 V (vs.

Research Article
doi.org/10.1002/batt.202300498
Chemistry Europe
European Chemical Societies Publishing

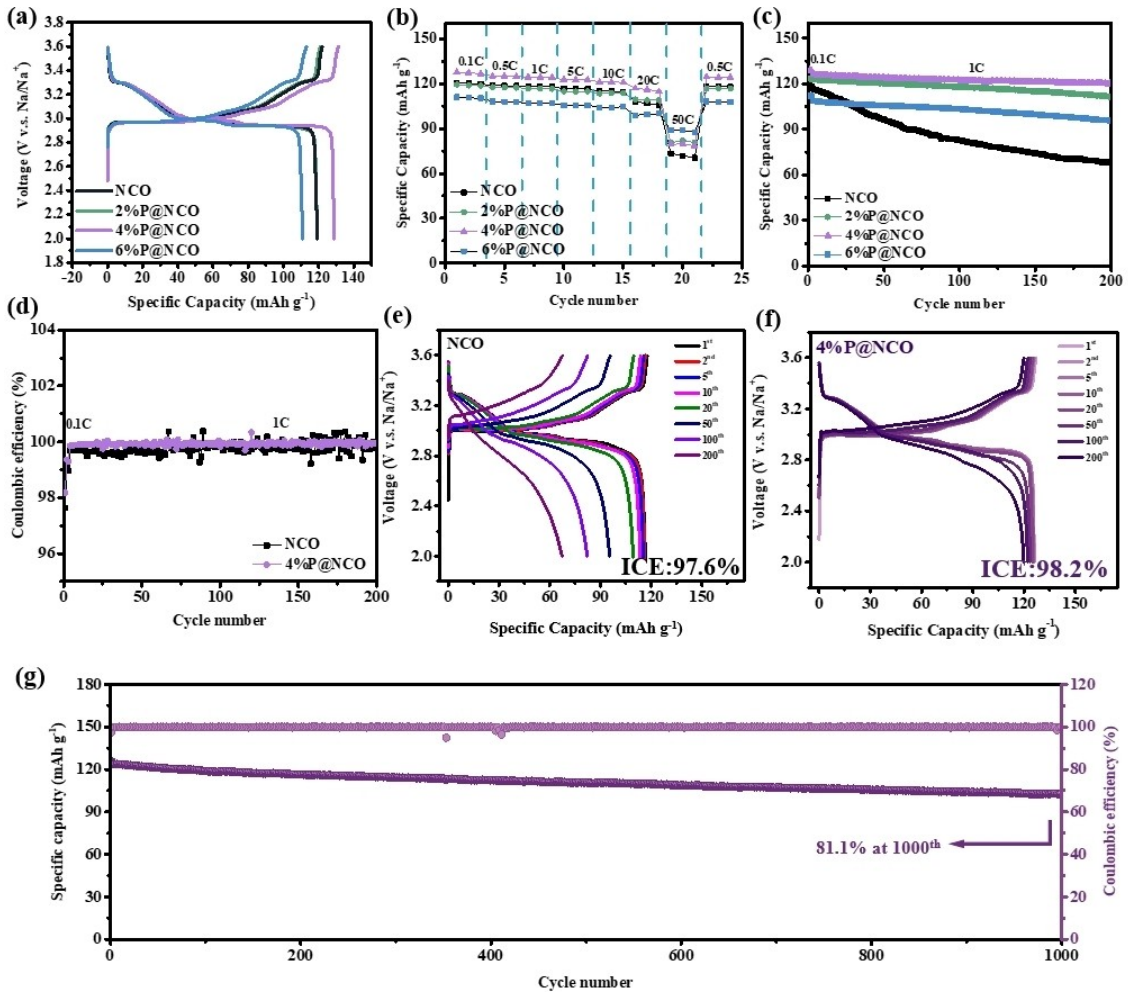

Figure 3. a) First cycle potential-capacity curves of NCO and x%P@NCO cycled in the voltage range of 2–3.6 V at a rate of 0.1 C, b) rate performance at various rates between 2 and 3.6 V. c) The cyclability of as prepared samples at 1 C. d) Coulombic efficiency of NCO and 4%P@NCO, Representative voltage profiles for e) NCO and f) 4%P@NCO, g) long-term cyclability of 4%P@NCO at 5 C.

Na/Na^+) and 3.34/3.28 V (vs. Na/Na^+) corresponding to the redox reaction of Cr^{3+}/Cr^{4+} which are well consistent with the voltage profiles and previous reports.[49] The remaining small peaks represent reversible phase transitions or sodium/vacancy ordering that occur during the reaction. The CV curves of the three coated materials are similar to that of raw NCO, and the calculation of the potential difference of the oxidation-reduction potential ($\triangle V$) are marked in Figure 4. It is found that with the increase of asphalt, the polarization gradually decreases and the reversibility increases.

Figure S7 shows the CV curves of the four materials prepared for the first three turns at 0.1 $mV s^{-1}$. The potential difference values ($\triangle V$) are recorded in Table S3. Generally, the polarization decreases as the amount of coating increases, which is compelling evidence that the coating is effective in maintaining the stability of the materials. Furthermore, it is found that the CV response current and potential position hardly change during the cycles, showing excellent reversibility and redox kinetics. Meanwhile, according to the power law relation $i = av^b$,[50] the storage mechanism and capacitance contribution of 4%P@NCO are studied. As shown in Figure S8, the b value is between 0.57 and 0.99. It has been reported that the b value of 0.5 indicates a semi-infinite linear diffusion limited redox reaction, while the b value of 1 means a fast surface-controlled pseudocapacitive process.[51,52] Thus, diffusion control and pseudocapacitance behavior are jointly involved in the 4%P@NCO redox process, which is thought to be conducive to fast kinetics related to the rate properties of the material.

In order to compare the influence of asphalt coating on ion migration dynamics, GITT tests were conducted on NCO and 4%P@NCO. The GITT curve of 4%P@NCO and the sodium ion diffusion coefficient (D_{Na+}) corresponding to the current pulse are shown in Figure 4(c), and the corresponding curve of NCO is shown in Figure S9. D_{Na+} is calculated according to the following formula to obtain [Equation (1)]:[53]

$$D_{Na^+} = \frac{4}{\pi\tau}\left(\frac{n_m V_m}{S}\right)^2\left(\frac{\Delta E_s}{\Delta E_\tau}\right)^2 \quad (1)$$

As shown in the local magnification of the current pulse in Figure S10, τ, n_m, V_m, and S are the duration of current pulse during the test, the number of moles of materials, the molar

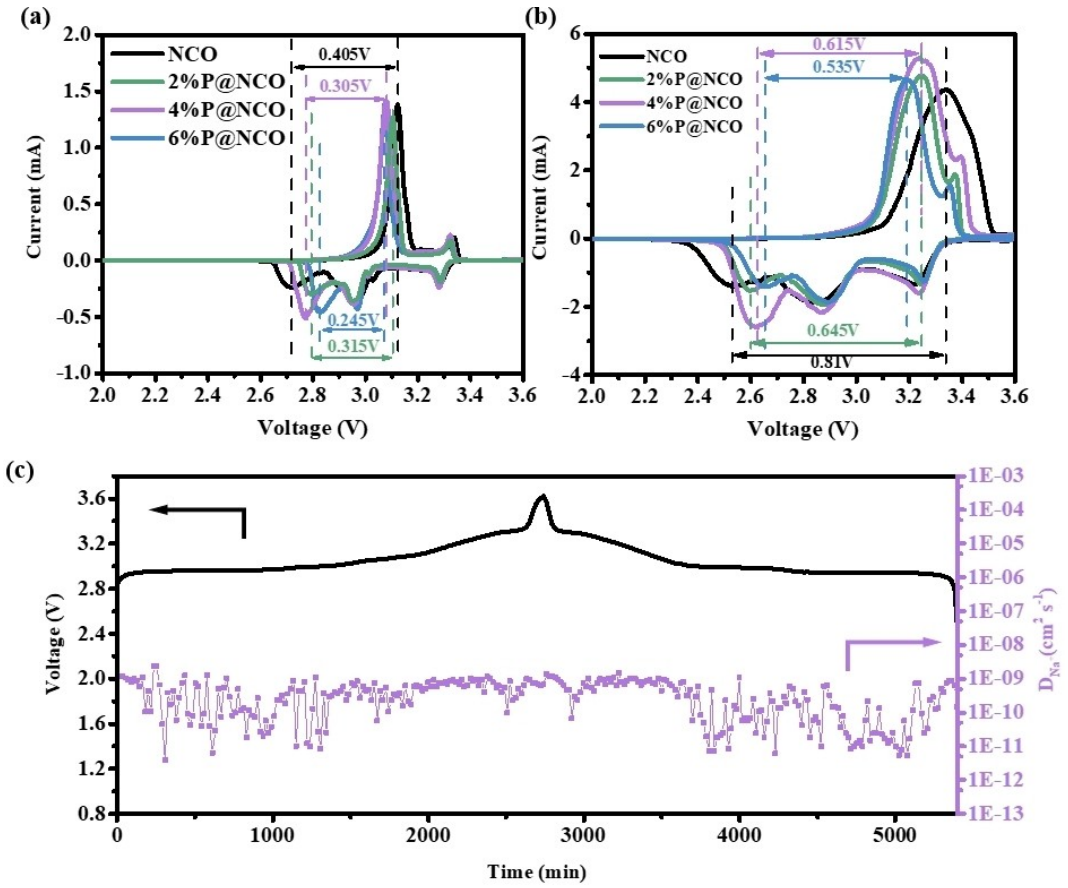

Figure 4. CV curves of $NaCrO_2$ and *x*%P@NCO at a) 0.1 mV s^{-1} and b) 1 mV s^{-1}, c) GITT profile and Na^+ diffusion coefficients of 4%P@NCO.

volume of the active materials and the effective area of the electrode, respectively. $\triangle E_s$ represents the variation of cell voltage during a constant current charge and discharge. $\triangle E_\tau$ is the variation of cell voltage during a constant current charge and discharge. The calculated average D_{Na+} value of 4%P@NCO (4.46×10^{-10} $cm^2 s^{-1}$) is higher than that of NCO (3.72×10^{-10} $cm^2 s^{-1}$). A higher diffusion coefficient indicates the easier diffusion of sodium ions in the material, leading to excellent high rate performance.

The low temperature performance of NCO and 4%P@NCO were shown in Figure 5(a and b). The coated material shows better rate and cycling performance than NCO even at −20 °C, with a high capacity of 119.1 mAh g^{-1} at 1 C, and the capacity retention rate is 76.4% after 150 cycles, which proves that the material is not affected by low temperature environment. It makes the material has great significance in special environment applications. The coated 4%P@NCO also shows decent cycling performance in high temperature performance tests at 50 °C, as shown in Figure S11. In addition, the XRD of NCO and 4%P@NCO material before and after 200 cycles were compared (Figure 5c). It can be observed that the peak position of the bare NCO sample shifted obviously to lower angle after cycles, while the XRD peak of 4%P@NCO hardly move. The shift of XRD peaks of NCO materials is ascribed to the gradual loss of Na^+ in the material leading to the collapse of O3 structure during cycling. It also proves that the addition of asphalt can improve the cyclic performance of the material by slowing down the phase transition caused by the cycle. In order to investigate the air stability of 4%P@NCO, XRD characterization of materials exposed to air were conducted and shown in Figure S12(a). It shows that 4%P@NCO sample exposed to air displayed the same structure as untreated 4%P@NCO. Figure S12(b and c) shows the exposed sample has the same charging and discharging platform as the untreated sample and similar cycle performance. The electrochemical impedance (EIS) of the two materials after 200 cycles was tested, as shown in Figure S13, and the equivalent circuit after fitting is shown in the illustrations. The spectra of both materials show two semicircles, the high frequency semicircle represents the diffusion conduction process of sodium ions and the interface resistance of the CEI layer, while the low frequency semicircle represents the charge transfer resistance. In addition, the charge transfer resistance R_{ct} of 4%P@NCO is much smaller than that of NCO, suggesting that asphalt coating is conducive to surface reaction and promotes the transfer of sodium ions.[35,54] Specific fitting data are listed in Tables S4 and S5.

In addition, we assembled coin-type full cells using 4% P@NCO cathode with commercial hard carbon anode and conducted electrochemical tests to evaluate the practical potential of the material.[18,55] As shown in Figure S14, it is found that the battery performance was poor when assembled with the electrolyte used $NaClO_4$ as solvent, therefore the full cells

Research Article
doi.org/10.1002/batt.202300498
Chemistry Europe
European Chemical Societies Publishing

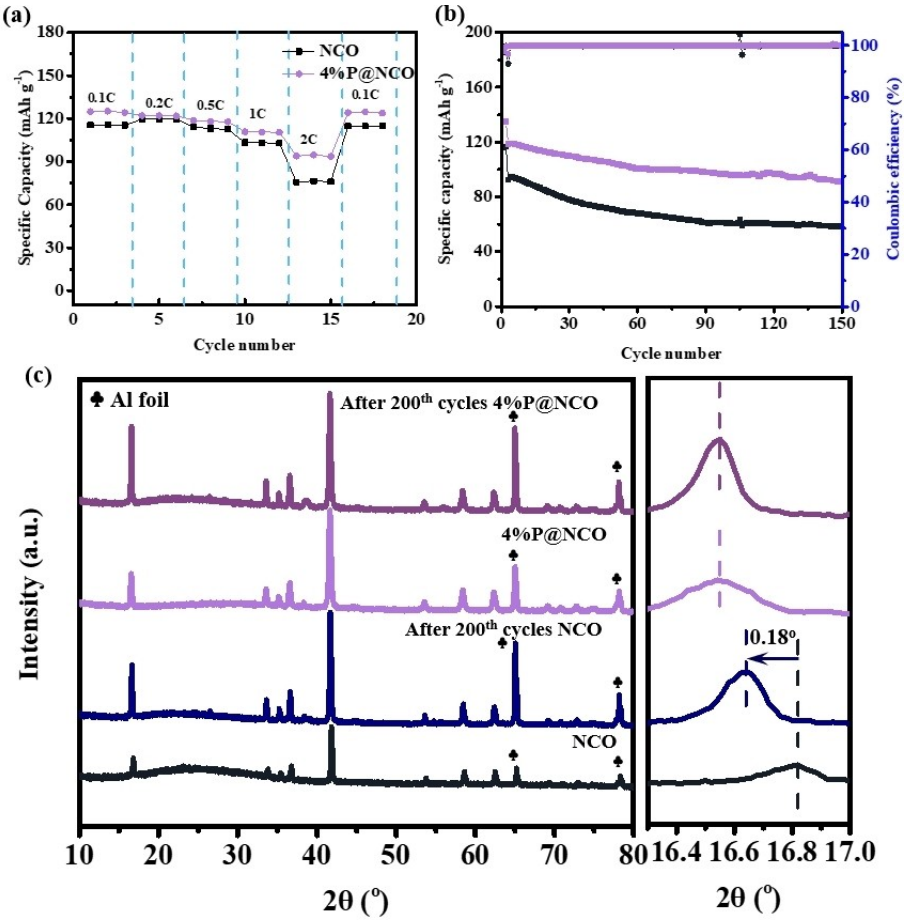

Figure 5. a) Comparison of rate performance at various rates and b) the cyclability at 1 C of NCO and 4%P@NCO between 2 and 3.6 V at −20 °C. c) *Ex situ* XRD patterns of bare electrode and 4%P@NCO electrode after 200 cycles.

were assembled with 1.0 M $NaPF_6$ as solvent in EC:DMC:EMC = 1:1:1 Vol % electrolyte according to Figure 6(a).The initial charge and discharge curve of the 4%P@NCO/HC full cell (green) and the activation curve of the HC/Na half cell (black) at 0.1 C under the voltage range 0.01–2 V are shown in Figure 6(b). The first cycle of the full cell shows a charge/discharge capacity of 128.7/121.9 mAh g^{-1}, with a high Coulomb efficiency of 94.7% and an average operating voltage of about 2.9 V at discharge process. In Figure 6(c), the battery can work normally at the increasing current density of 0.1 C-3 C. In addition, Figure 6**(d)** shows that the full cell can carry out high coulombic efficiency cycles at 1 C current density and the capacity can remain above 80% after 100 cycles. This demonstrates the excellent electrochemical properties of 4%P@NCO/HC full cell.

Conclusions

In summary, a serious of O3-typed carbon-coated cathodes (*x*% P@NCO) were successfully constructed by a simple one-step synthesis method. The cells with 4%P@NCO cathode show a high specific capacity of 129 mAh g^{-1} at 0.1 C, excellent rate performance and significant cyclability. After 1000 cycles under 5 C current density, material's capacity still has 102.8 mAh g^{-1} and the retention rate is 81.1%. We successfully proved through XPS and *ex situ* XRD tests that asphalt can improve the air stability. Consequently, the irreversible phase transition caused by charge and discharge is inhibited, the stability of the interface is improved, and the spacing between layers is enlarged, hence facilitates the sodium ions transport. Even at −20 °C temperature, the material can still maintain the discharge specific capacity consistent with room temperature. The full cell of 4%P@NCO was assembled and tested, showing that the specific capacity, rate and cycle performance meet the practical application. Therefore, this work provides a new coating idea for the performance improvement of $NaCrO_2$ and makes a preliminary exploration of surface forming materials, which is of great significance for the subsequent work.

Experimental Section

The O3-type $NaCrO_2$ and P@NCO powders were synthesized by a simple solid state reaction using *in situ* coating method. The raw materials Na_2CO_3 (Aladdin, purity > 99.5%) (an additional 5 wt% were added due to the volatility at high temperatures) and Cr_2O_3 (Macklin, purity > 99.0%) were ball milled and mixed according to the molar ratio. On the basis of the two raw precursors, 2 wt%, 4 wt % and 6 wt% asphalt were added as carbon source in the ball

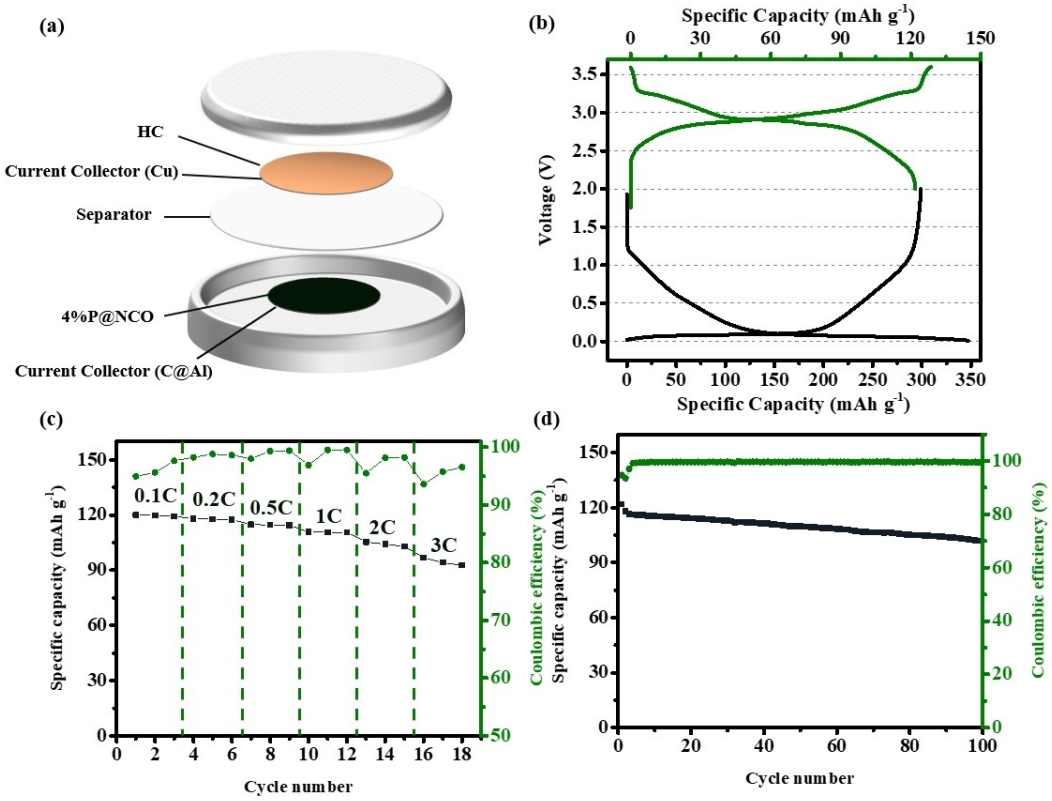

Figure 6. Electrochemical performance of the 4%P@NCO/HC sodium ion full cell. a) Schematic diagram of the construction of a sodium ion full cell used here, b) first cycle potential-capacity curve at 0.1 C rate over the potential range of 2–3.6 V for NCO and 0.01–2 V for presodiated HC vs. Na metal, c) the rate behaviors at various rates as indicated, d) cycle behavior of the full cell at 1 C.

milling process, and the resulting materials were expressed as *x*% P@NCO ($x=2$, 4, 6). Ball milling was conducted for 30 min at 1500 rpm. All mixtures were pressed into circular pellets at a pressure of 15 MPa, and then heated to 900 °C with a heating rate of 5 °C min^{-1} in nitrogen atmosphere for 12 hours to obtain the final samples. The samples were immediately transferred into the glove box for preservation to avoid the influence of air and moisture. In addition, the detailed materials characterization and electrochemical measurements are summarized in Supporting Information.

Acknowledgements

This work was financially supported by National Natural Science Foundation of China (NSFC 52374302 and 51874099), National Science Foundation of Fujian Province's Key Project (2021J02031), Natural Science Foundation of Fujian Province (2023J01518) and Education Department of Fujian Province (JAT210054). Z.H. also thanks the support from the open fund from Academy of Carbon Neutrality of Fujian Normal University (TZH2022-06).

Conflict of Interests

The authors declare no conflict of interest.

Data Availability Statement

The data that support the findings of this study are available from the corresponding author upon reasonable request.

Keywords: in-situ carbon coating · $NaCrO_2$ cathode · sodium-ion battery · sodium vacancy · structure modification

[1] J.-H. Kim, M.-J. Jung, M.-J. Kim, Y.-S. Lee, *J. Ind. Eng. Chem.* **2018**, *61*, 368.
[2] Y. P. Deng, Z. G. Wu, R. L. Liang, Y. Jiang, D. Luo, A. P. Yu, Z. W. Chen, *Adv. Funct. Mater.* **2019**, *29*, 1808522.
[3] X. M. Yang, A. L. Rogach, *Adv. Energy Mater.* **2020**, *10*, 2000288.
[4] J. Xiao, X. Li, K. K. Tang, D. D. Wang, M. Q. Long, H. Gao, W. H. Chen, C. T. Liu, H. Liu, G. X. Wang, *Mater. Chem. Front.* **2021**, *5*, 3735.
[5] Y. Yuan, Z. W. Chen, H. X. Yu, X. K. Zhang, T. T. Liu, M. T. Xia, R. T. Zheng, M. Shui, J. Shu, *Energy Storage Mater.* **2020**, *32*, 65.
[6] J. Y. Hwang, S. T. Myung, Y. K. Sun, *Chem. Soc. Rev.* **2017**, *46*, 3529.
[7] D. R. Lide, *CRC handbook of chemistry and physics*; CRC press, 2004; Vol. 85.
[8] H. Y. Kang, Y. C. Liu, K. Z. Cao, Y. Zhao, L. F. Jiao, Y. J. Wang, H. T. Yuan, *J. Mater. Chem. A.* **2015**, *3*, 17899.
[9] R. M. Gao, Z. J. Zheng, P. F. Wang, C. Y. Wang, H. Ye, F. F. Cao, *Energy Storage Mater.* **2020**, *30*, 9.
[10] Q. Li, S. Xu, S. Guo, K. Jiang, X. Li, M. Jia, P. Wang, H. Zhou, *Adv. Mater.* **2020**, *32*, 1907936.
[11] J. Darga, J. Lamb, A. Manthiram, *Energy Technol.* **2020**, *8*, 2000723.
[12] P. K. Nayak, L. Yang, W. Brehm, P. Adelhelm, *Angew. Chem. Int. Ed.* **2018**, *57*, 102.
[13] Q. Liu, Z. Hu, M. Chen, C. Zou, H. Jin, S. Wang, S. L. Chou, S. X. Dou, *Small.* **2019**, *15*, 1805381.
[14] J. Q. Deng, W. B. Luo, X. Lu, Q. R. Yao, Z. M. Wang, H. K. Liu, H. Y. Zhou, S. X. Dou, *Adv. Energy Mater.* **2018**, *8*, 1701610.

[15] J. Liang, L. Liu, X. Liu, X. Meng, L. Zeng, J. Liu, J. Li, Z. Shi, Y. Yang, *ACS Appl. Mater. Interfaces.* **2021**, *13*, 22635.
[16] S.-H. Bo, X. Li, A. J. Toumar, G. Ceder, *Chem. Mater.* **2016**, *28*, 1419.
[17] Y. N. Zhou, J. J. Ding, K. W. Nam, X. Q. Yu, S. M. Bak, E. Y. Hu, J. Liu, J. M. Bai, H. Li, Z. W. Fu, X. Q. Yang, *J. Mater. Chem. A.* **2013**, *1*, 11130.
[18] S. Komaba, C. Takei, T. Nakayama, A. Ogata, N. Yabuuchi, *Electrochem. Commun.* **2010**, *12*, 355.
[19] Q. Liu, Z. Hu, W. Li, C. Zou, H. Jin, S. Wang, S. Chou, S.-X. Dou, *Energy Environ. Sci.* **2021**, *14*, 158.
[20] J. H. Wu, G. R. Hu, K. Du, Z. D. Peng, M. Huang, J. Fan, Y. F. Gong, D. C. Guan, Y. Shi, R. R. Liu, Y. B. Cao, *Electrochim. Acta.* **2022**, *403*, 139641.
[21] H. Y. Lu, R. L. Hou, S. Y. Chu, H. S. Zhou, S. H. Guo, *Acta Phys-Chim Sin.* **2023**, *39*, 102950.
[22] L. T. Zheng, J. C. Bennett, M. N. Obrovac, *J. Electrochem. Soc.* **2019**, *166*, A2058.
[23] M. Matsui, F. Mizukoshi, N. Imanishi, *J. Power Sources.* **2015**, *280*, 205.
[24] W. Li, Y. Wang, G. R. Hu, Z. D. Peng, Y. B. Cao, Y. X. Zeng, K. Du, *J. Alloys Compd.* **2019**, *779*, 147.
[25] Y. S. Wang, P. X. Cui, W. Zhu, Z. M. Feng, M. J. Vigeant, H. Demers, A. Guerfi, K. Zaghib, *J. Power Sources.* **2019**, *435*, 226760.
[26] J. J. Ding, Y. N. Zhou, Q. Sun, Z. W. Fu, *Electrochem. Commun.* **2012**, *22*, 85.
[27] A. Bhardwaj, A. K. Panwar, *Appl. Surf. Sci.* **2022**, *573*, 151449.
[28] S. Wang, F. Chen, T. Y. Zhu, X. D. He, J. Y. Liao, L. M. Zhang, X. Ding, Q. Hu, C. H. Chen, *ACS Appl. Mater. Interfaces* **2020**, *12*, 44671.
[29] A. B. Ikhe, W. B. Park, M. Manasi, D. Ahn, K. S. Sohn, M. Pyo, *ACS Appl. Mater. Interfaces.* **2023**, *15*, 14958.
[30] C. H. Lin, X. C. Meng, M. Liang, W. Y. Li, J. J. Liang, T. F. Liu, X. Ke, J. Liu, Z. C. Shi, L. Y. Liu, *J. Mater. Chem. A.* **2023**, *11*, 68.
[31] J. Y. Liao, Q. Hu, X. R. Sheng, Z. Z. Zhang, Y. F. Xu, X. Y. Mo, X. S. Zhou, *ACS Materials Lett.* **2022**, *4*, 1653.
[32] Z. Z. Zhang, Q. Hu, J. Y. Liao, Y. F. Xu, R. Q. Tian, Y. C. Du, J. Shen, X. S. Zhou, *Nano Lett.* **2023**, *23*, 694.
[33] L. P. Duan, H. W. Tang, X. F. Xu, J. Y. Liao, X. D. Li, G. M. Zhou, X. S. Zhou, *Energy Storage Mater.* **2023**, *62*, 102950.
[34] X. G. Yuan, Y. J. Guo, L. Gan, X. A. Yang, W. H. He, X. S. Zhang, Y. X. Yin, S. Xin, H. R. Yao, Z. G. Huang, Y. G. Guo, *Adv. Funct. Mater.* **2022**, *32*, 2111466.
[35] B. X. Ouyang, T. Chen, X. C. Liu, M. J. Zhang, P. G. Liu, P. L. Li, W. F. Liu, K. Y. Liu, *Chem. Eng. J.* **2023**, *458*, 141384.
[36] N. Voronina, M. Y. Shin, H. J. Kim, N. Yaqoob, O. Guillon, S. H. Song, H. Kim, H. D. Lim, H. G. Jung, Y. Kim, H. K. Lee, K. S. Lee, K. Yazawa, K. Gotoh, P. Kaghazchi, S. T. Myung, *Adv. Energy Mater.* **2022**, *12*, 2103939.
[37] S. C. Han, H. Lim, J. Jeong, D. Ahn, W. B. Park, K.-S. Sohn, M. Pyo, *J. Power Sources.* **2015**, *277*, 9.
[38] T. Chen, W. F. Liu, Y. Zhuo, H. Hu, J. Guo, Y. C. Liu, J. Yan, K. Y. Liu, *Chem. Eng. J.* **2020**, *383*, 123087.
[39] Y. S. Li, X. M. Li, C. C. Du, H. M. Sun, Y. Zhang, Q. A. Liu, T. T. Yang, J. Zhao, C. Delmas, S. J. Harris, H. L. Chen, Q. Huang, Y. F. Tang, L. Q. Zhang, T. Zhu, J. Y. Huang, *ACS Energy Lett.* **2021**, *6*, 3960.
[40] H. Estrade-Szwarckopf, B. Rousseau, C. Herold, P. Lagrange, *Mol. Cryst. Liq. Cryst. Sci. Technol. Sect. A* **2006**, *310*, 231.
[41] C. Van Vuuren, *Thermochim. Acta.* **1990**, *168*, 135.
[42] S. Lee, W. Jin, S. H. Kim, S. H. Joo, G. Nam, P. Oh, Y. K. Kim, S. K. Kwak, J. Cho, *Angew. Chem. Int. Ed.* **2019**, *58*, 10478.
[43] H. P. Wang, C. L. Zhu, J. D. Liu, S. H. Qi, M. G. Wu, J. D. Huang, D. X. Wu, J. M. Ma, *Angew. Chem. Int. Ed.* **2022**, *61*, e202208506.
[44] D. X. Wu, C. L. Zhu, M. G. Wu, H. P. Wang, J. D. Huang, D. L. Tang, J. M. Ma, *Angew. Chem. Int. Ed.* **2022**, *61*, e202214198.
[45] K. Mathiyalagan, A. Ponnaiah, K. Karuppiah, S. Rengapillai, S. Marimuthu, *Ionics.* **2020**, *26*, 3929.
[46] H.-R. Yao, L. Zheng, S. Xin, Y.-G. Guo, *Science China Chemistry* **2022**, *65*, 1076.
[47] N. T. Aristote, K. Y. Zou, A. D. Di, W. T. Deng, B. W. Wang, X. L. Deng, H. S. Hou, G. Q. Zou, X. B. Ji, *Chin. Chem. Lett.* **2022**, *33*, 730.
[48] Y. K. Xu, H. Z. Sun, C. S. Ma, J. J. Gai, Y. H. Wan, W. H. Chen, *Chin. J. Chem. Eng.* **2021**, *39*, 261.
[49] C. L. Jakobsen, M. Brighi, B. P. Andersen, G. Ducrest, R. Černý, D. B. Ravnsbæk, *J. Power Sources* **2022**, *535*, 231317.
[50] F. Wang, N. Zhang, X. Zhao, L. Wang, J. Zhang, T. Wang, F. Liu, Y. Liu, L. Z. Fan, *Adv. Sci.* **2019**, *6*, 1900649.
[51] G. Wang, N. Chandrasekhar, B. P. Biswal, D. Becker, S. Paasch, E. Brunner, M. Addicoat, M. Yu, R. Berger, X. Feng, *Adv. Mater.* **2019**, *31*, 1901478.
[52] Z. Q. Sun, K. J. Zhu, P. Liu, H. X. Li, L. F. Jiao, *Adv. Funct. Mater.* **2021**, *31*, 2107830.
[53] S. Wang, F. Chen, X. D. He, L. M. Zhang, F. Chen, J. R. Wang, J. M. Dong, C. H. Chen, *ACS Appl. Mater. Interfaces* **2021**, *13*, 12203.
[54] M. Matsui, F. Mizukoshi, H. Hasegawa, N. Imanishi, *J. Power Sources* **2021**, *485*, 229346.
[55] J. A. S. Oh, G. Deysher, P. Ridley, Y. T. Chen, D. Cheng, A. Cronk, S. Y. Ham, D. H. S. Tan, J. Jang, L. H. B. Nguyen, Y. S. Meng, *Adv. Energy Mater.* **2023**, *13*, 2300776.

Manuscript received: October 23, 2023
Revised manuscript received: November 28, 2023
Accepted manuscript online: November 29, 2023
Version of record online: December 13, 2023